Distinguishing finite-momentum superconducting pairing states with two-electron photoemission spectroscopy

Fahad Mahmood,[1,2] Thomas Devereaux,[3,4] Peter Abbamonte,[1,2] and Dirk K. Morr[5]
[1]*Department of Physics, University of Illinois at Urbana-Champaign, Urbana, Illinois 61801, USA*
[2]*Materials Research Laboratory, University of Illinois at Urbana-Champaign, Urbana, Illinois 61801, USA*
[3]*Department of Materials Science and Engineering, Stanford University, Stanford, California 94305, USA*
[4]*Stanford Institute for Materials and Energy Sciences, SLAC National Accelerator Laboratory, Menlo Park, California 94025, USA*
[5]*Department of Physics, University of Illinois at Chicago, Chicago, Illinois 60607, USA*

(Received 9 August 2021; revised 4 January 2022; accepted 2 February 2022; published 25 February 2022)

We show theoretically that double photoemission (2*e*-ARPES) may be used to identify the pairing state in superconductors in which the Cooper pairs have a nonzero center-of-mass momentum, $\mathbf{q}_{\rm cm}$. We theoretically evaluate the 2*e*-ARPES counting rate $P^{(2)}$ for the cases of a $d_{x^2-y^2}$-wave superconductor, a pair-density-wave (PDW) phase, and a Fulde-Ferrel-Larkin-Ovchinnikov (FFLO) phase. We show that $P^{(2)}$ provides direct insight into the center-of-mass momentum and spin state of the superconducting condensate, and thus can distinguish between these three different superconducting pairing states. In addition, $P^{(2)}$ can be used to map out the momentum dependence of the superconducting order parameter. Our results identify 2*e*-ARPES as an ideal tool for identifying and probing $\mathbf{q}_{\rm cm} \neq 0$ superconducting pairing states in superconductors.

DOI: 10.1103/PhysRevB.105.064515

I. INTRODUCTION

Identifying the pairing symmetries of unconventional superconductors has remained one of the most important and fundamental challenges in quantum materials research. Its difficulty arises from the absence of two-particle spectroscopies that directly probe the properties of the Cooper pair wave function, which determine the spin structure and momentum dependence of the superconducting order parameter. Single-particle spectroscopies such as tunneling [1] or angle-resolved photoemission spectroscopy (ARPES) [2] can only measure the magnitude of the superconducting order parameter (or the gap) but not its phase, while macroscopic Josephson interference measurements can probe its phase, but only if the order parameter is spatially uniform and suitable junctions can be prepared [3,4]. The difficulties are even more acute for superconductors in which the Cooper pairs possess a nonzero center-of-mass momentum $\mathbf{q}_{\rm cm}$, such as the Fulde-Ferrel-Larkin-Ovchinnikov (FFLO) phase [5,6] or the predicted pair density wave (PDW) [7], in which the superconducting order parameter is modulated in real space.

In this paper, we demonstrate that two electron coincidence spectroscopy (2*e*-ARPES), in which the absorption of a single photon leads to the emission of two coincident photoelectrons [8], can directly reveal the microscopic character of finite-momentum pairing states in superconductors. The experimental 2*e*-ARPES signal, the photoelectron counting rate $P^{(2)}$, which is related to a two-particle spectral function [9], is the probability per unit time that a single photon leads to the emission of a correlated pair of photoelectrons with defined energy and momentum, as measured by two separate detectors. Moreover, as spin filters in the form of 3D spin VLEED or Mott detectors can be employed to identify the spin state of each electron independently, 2*e*-ARPES experiments can measure a spin-dependent $P^{(2)}$. We show theoretically that the $d_{x^2-y^2}$-wave superconducting, FFLO and PDW phases have distinct spectroscopic signatures in $P^{(2)}$ that are directly sensitive to the center-of-mass momentum and spin state of the Cooper pair wave function. 2*e*-ARPES is therefore a promising technique for identifying and studying spatially modulated superconductors generally.

There are two distinct processes that can cause a single photon to lead to the ejection of a correlated pair of electrons [Figs. 1(a) and 1(b)] [8,10–16]. In the first, the photon is absorbed and excites a valence band electron into a free photoelectron state, which subsequently ejects a second valence electron via an electron energy-loss (EELS)-like scattering event [Fig. 1(a)]. In the second process, the first photoelectron is excited from a core-level, which is subsequently filled by a valence electron, leading to the emission of a second valence electron through an Auger process [Fig. 1(b)]. While both processes lead to a very similar energy, momentum and spin dependence of $P^{(2)}$ (see Appendices A and B), the use of lower photon energy, laser based XUV sources will not allow 2*e*-ARPES experiments to directly probe core states, rather rendering them more sensitive to valence band effects. We thus restrict our theoretical analysis to first type of process, shown in Fig. 1(a).

II. THEORETICAL FORMALISM

We compute the 2*e*-ARPES photoelectron counting rate $P^{(2)}$ in the sudden approximation whereby we neglect relaxation pathways during the photoelectron emission process and

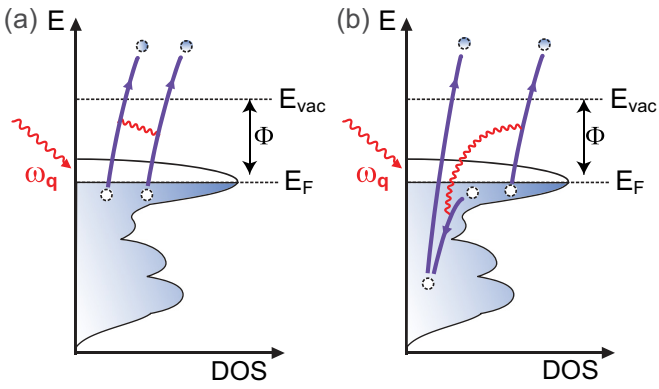

FIG. 1. Schematic representation of the two distinct $2e$-ARPES processes involving the absorption of a single photon, and the ejection of two photoelectrons. (a) The incident photon excites a valence electron into a free photoelectron state with $E > E_{\text{vac}}$, which in turn ejects a second valence electron through an EELS-like scattering event. Here, $E_{\text{vac}} = E_F + \Phi$, where E_F is the Fermi energy and Φ is the work function. (b) The incident photon excites an electron from a core level which is then filled by a valence electron, emitting a second valence electron though an Auger process.

work with plane wave electrons at the detector and valence electron states in a sample [17]. As mentioned above, we focus on the two-step process shown in Fig. 1(a) involving the emission of a first photoelectron upon absorption of a photon, and the subsequent scattering (EELS-like) process between the emitted photoelectron and a conduction electron, which leads to the emission of a second photoelectron. We assume that the scattering process between the photoelectron and conduction electron is mediated by a (screened) Coulomb interaction. This entire process is then described by the Hamiltonian

$$H_{\text{sc}} = \sum_{\mathbf{k},\mathbf{q},\sigma,\nu} \gamma_\nu(\mathbf{q}) d^\dagger_{\mathbf{k}+\mathbf{q},\sigma} c_{\mathbf{k},\sigma} (a_{\mathbf{q},\nu} + a^\dagger_{-\mathbf{q},\nu}) + \sum_{\mathbf{k},\mathbf{p},\mathbf{q},\alpha,\beta} V(\mathbf{q}) d^\dagger_{\mathbf{k}+\mathbf{q},\alpha} d^\dagger_{\mathbf{p}-\mathbf{q},\beta} d_{\mathbf{p},\beta} c_{\mathbf{k},\alpha} + \text{H.c.} \quad (1)$$

Here, $\gamma_\nu(\mathbf{q})$ is the effective electron-photon dipole interaction, $d^\dagger_{\mathbf{k},\sigma}(c_{\mathbf{k},\sigma})$ creates (destroys) a photoelectron (conduction electron) with momentum $\mathbf{k}$ and spin σ, and $V(\mathbf{q}) = V_0/(\mathbf{q}^2 + \kappa^2)$ is the Fourier transform of the (screened) Coulomb interaction, with κ^{-1} being the screening length. For all results shown below, we consider for concreteness $\kappa^{-1} = 10a_0$ (see also Appendix C). Moreover, since the photon momentum is much smaller than typical fermionic momenta, we set it equal to zero, and as the out-of-plane momentum is not conserved upon absorption of the photon, we take $\gamma_\nu(\mathbf{q}) = \gamma_0$ to be independent of the in-plane momentum. We note that due to the coupling of photoelectrons and conduction electrons via the Coulomb interaction, the actual electron operators are a superposition of photoelectron operators and conduction electron operators. The Coulomb interaction is given in terms of the actual electron operators, which then yields the form of the Coulomb interaction presented in Eq. (1) above. There are of course other terms that arise from writing the actual electron operators in terms of the photoelectron and conduction electron operators (such as terms containing $2c$ and $2d$ operators or $1d$ and $3c$ operators), but these terms are irrelevant for the $2e$-ARPES scattering process.

The initial and final states of the entire system, $|\Psi_a\rangle$ and $|\Psi_b\rangle$, respectively, are described by

$$|\Psi_a\rangle = |\Phi_a\rangle|1_{\mathbf{q},\lambda}\rangle_p|0\rangle_{pe},$$
$$|\Psi_b\rangle = |\Phi_b\rangle|0\rangle_p|1_{\mathbf{k}'_1,\sigma'_1}1_{\mathbf{k}'_2,\sigma'_2}\rangle_{pe}. \quad (2)$$

Here, $|1_{\mathbf{q}\lambda}\rangle_p$ describes the initial photon state containing one photon with momentum $\mathbf{q}$ and polarization λ, and $|1_{\mathbf{k}'_1,\sigma'_1}1_{\mathbf{k}'_2,\sigma'_2}\rangle_{pe}$ represents the final photoelectron state containing two photoelectrons with momenta $\mathbf{k}'_{1,2}$ and spin $\sigma'_{1,2}$. The initial and final states of the superconductor are described by $|\Phi_{a,b}\rangle$, respectively. The $2e$-ARPES signal, which depends on the two photoelectron momenta and spin projections, is then computed via

$$P^{(2)}(\mathbf{k}'_1,\sigma'_1,\mathbf{k}'_2,\sigma'_2) = \frac{1}{Z}\sum_{a,b}\frac{e^{-\beta E_a}}{\Delta t}|\langle\Psi_b|\hat{S}^{(2)}(\infty,-\infty)|\Psi_a\rangle|^2 \quad (3)$$

where Z is the partition function, the sum runs over all states $|\Phi_{a,b}\rangle$ of the superconductor, Δt is the time over which the photon beam is incident in the superconductor, and $\hat{S}^{(2)}$ is the second-order contribution to the S matrix arising from H_{sc}. The detailed derivation of $P^{(2)}$ for a uniform $d_{x^2-y^2}$-wave superconductor, the PDW and the FFLO phases is carried out in Appendix A. While we consider for concreteness a cupratelike Fermi surface, as shown in Fig. 2(a), our results shown below are quite general and applicable to a wide variety of superconductors with varying Fermi surface structure.

III. RESULTS

We begin by discussing the case of a uniform, spin-singlet $d_{x^2-y^2}$-wave superconductor (band parameters are given in Appendix A) in which the Cooper pairs possess a zero center of mass momentum. For $P^{(2)}$ to directly probe the superconducting condensate, we need to require that the two photoelectrons have a zero center-of-mass momentum, i.e., $\mathbf{k}'_2 = -\mathbf{k}'_1$, and opposite spins, i.e., $\sigma'_2 \neq \sigma'_1$. In this case, we obtain $P^{(2)} = P^{(2)}_{\text{SC}} + P^{(2)}_{\text{2cp}}$ where (at $T = 0$)

$$P^{(2)}_{\text{SC}} = 2\pi\delta(\omega_q - 2\varepsilon_{\mathbf{k}'_1})\left|\sum_{\mathbf{k}}\frac{\gamma_0 V(\mathbf{k}-\mathbf{k}'_1)}{\omega_q - E_{\mathbf{k}} - \varepsilon_{\mathbf{k}} + i\delta}\frac{\Delta_{\mathbf{k}}}{2E_{\mathbf{k}}}\right|^2,$$
$$P^{(2)}_{\text{2cp}} = 2\pi\sum_{\mathbf{k}}\left|\frac{\gamma_0 V(\mathbf{k}-\mathbf{k}'_1)v^2_{\mathbf{k}}}{\omega_q + E_{\mathbf{k}} - \varepsilon_{\mathbf{k}} + i\delta}\right|^2\delta(\omega_q - 2\varepsilon_{\mathbf{k}'_1} - 2E_{\mathbf{k}}), \quad (4)$$

where $E_{\mathbf{k}} = \sqrt{\xi^2_{\mathbf{k}} + \Delta^2_{\mathbf{k}}}$ ($\xi_{\mathbf{k}}$) is the conduction electron dispersion in the superconducting (normal) state, $v^2_{\mathbf{k}} = [1 - \xi_{\mathbf{k}}/E_{\mathbf{k}}]/2$, ω_q is the incident photon energy, and $\varepsilon_{\mathbf{k}'_1}$ is the sum of the kinetic energy and work function of a photoelectron. $\Delta\omega = \omega_q - 2\varepsilon_{\mathbf{k}'_1}$ represents the excess energy of the photon over the energies of the two photoelectrons. The first term, $P^{(2)}_{\text{SC}}$, directly reflects the existence of a superconducting condensate, as described by $\Delta_{\mathbf{k}}$, and arises from the breaking and subsequent creation of a Cooper pair. This term vanishes in the

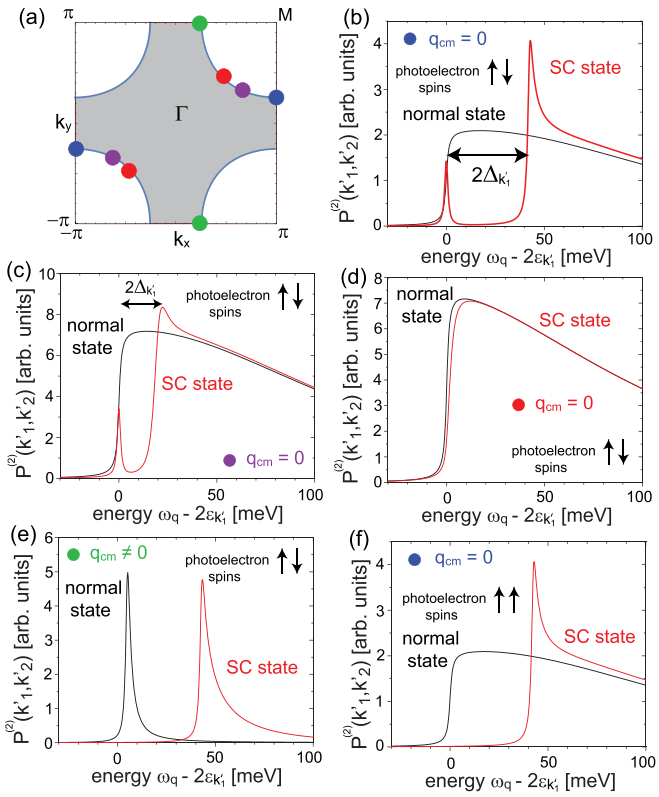

FIG. 2. (a) Fermi surface of the cuprate superconductors. [(b)–(d)] $P^{(2)}$ in a $d_{x^2-y^2}$-wave superconductors for two photoelectrons with opposite momenta $\mathbf{k}'_2 = -\mathbf{k}'_1$ along the Fermi surface, as indicated by the set of filled circles in (a), and opposite spins, $\sigma'_1 \neq \sigma'_2$. $P^{(2)}$ for photoelectrons (e) with momenta indicated by green circles and opposite spins, and (f) with momenta indicated by blue circles and equal spins.

normal state, and is absent when the two detected photoelectrons do not possess the same center of mass momentum, or spin structure as the superconducting condensate. As such, the photoelectron pairs that contribute to $P^{(2)}_{\rm SC}$ reside in an entangled state and are therefore Einstein-Podolsky-Rosen (EPR) pairs. Note that the momentum dependence of the Coulomb interaction plays a crucial role in observing a nonzero $P^{(2)}_{\rm SC}$ in a $d_{x^2-y^2}$-wave superconductor since for a momentum independent $V(\mathbf{q})$, $P^{(2)}_{\rm SC}$ vanishes identically due to the symmetry of the $d_{x^2-y^2}$-wave order parameter. In contrast, the photoelectron pairs that contribute to the second term, $P^{(2)}_{\rm 2cp}$, arise from the breaking of two Cooper pairs. As $P^{(2)}_{\rm 2cp}$ is weighted by the particlelike coherence factors of the broken Cooper pairs, i.e., $(v^2_{\mathbf{k}})^2$, it does not vanish in the normal state. Note that $P^{(2)}_{\rm SC}$ in Eq. (4) scales as N^2 (where N is the number of sites in the system), while $P^{(2)}_{\rm 2cp}$ scales as N. This difference arises since $P^{(2)}_{\rm SC}$ describes the breaking of a single Cooper pair, while $P^{(2)}_{\rm 2cp}$ describes that of two Cooper pairs, with the probability of finding a second Cooper pair scaling as $\sim 1/N$. To plot $P^{(2)}_{\rm SC}$ and $P^{(2)}_{\rm 2cp}$ in the same graph, as shown below, we have scaled them with overall factors of $(4\pi^2/N)^2$ and $4\pi^2/N$, respectively.

In Fig. 2(b), we present $P^{(2)}$ in the normal and superconducting state for opposite photoelectron momenta $\mathbf{k}'_2 = -\mathbf{k}'_1$ near the antinodal points [indicated by the filled blue circles in Fig. 2(a)]. In the normal state, $P^{(2)}$ shows an onset at $\Delta\omega = 0$, as conduction electrons can be excited from the filled Fermi sea for $\Delta\omega \geqslant 0$. In contrast, in the superconducting state, $P^{(2)}$ exhibits two distinct features. The first one is a peak at $\Delta\omega = 0$, previously identified in Ref. [18], arising from $P^{(2)}_{\rm SC}$ in Eq. (4) that is a direct signature of the superconducting condensate, as discussed above. The second feature is a continuum, described by $P^{(2)}_{\rm 2cp}$, with onset energy $\Delta\omega_c \approx 2\Delta_{\mathbf{k}'_1}$ (we will refer to this contribution as the 2CP continuum). The latter immediately reveals that $P^{(2)}_{\rm 2cp}$ reflects the measurement of two photoelectrons arising from the breaking of 2 Cooper pairs, requiring an energy of $2\Delta_{\mathbf{k}'_1}$. That the gap between the condensate peak at $\Delta\omega = 0$ and the continuum is indeed $2\Delta_{\mathbf{k}'_1}$ is a direct consequence of the momentum dependence of the Coulomb interaction, $V(\mathbf{q})$, which suppresses large momentum transfers during the scattering process. As a result, the main contribution to $P^{(2)}_{\rm 2cp}$ arises from those momentum states $\mathbf{k}$ along the Fermi surface with $\mathbf{k} \approx \pm\mathbf{k}'_1$.

This result allows one to map out the momentum dependence of the superconducting gap (similar to conventional ARPES experiments [2]) by measuring the energy distance between the $\Delta\omega = 0$ peak arising from $P^{(2)}_{\rm SC}$, and the peak at $\Delta\omega \approx 2\Delta_{\mathbf{k}'_1}$ arising from $P^{(2)}_{\rm 2cp}$ as a function of $\mathbf{k}'_{1,2}$, as shown in Figs. 2(b)–2(d). As $\mathbf{k}'_{1,2}$ are moved along the Fermi surface from the antinodal points towards the nodal points, the peak in $P^{(2)}_{\rm 2cp}$ located at $\Delta\omega \approx 2\Delta_{\mathbf{k}'_1}$ moves down in energy as the superconducting $d_{x^2-y^2}$-wave gap decreases. For $\mathbf{k}'_{1,2}$ at the nodal points, $P^{(2)}$ in the superconducting state is nearly identical to that in the normal state, due to the vanishing superconducting gap. The small differences arise from the fact that the momentum sums in the calculation of $P^{(2)}$ [see Eq. (4)] probe a small momentum region in the vicinity of the nodal points where the superconducting gap is nonzero but small.

A qualitatively new feature of $2e$-ARPES is that it can be used to identify the center-of-mass momentum of the Cooper pairs, $\mathbf{q}_{\rm cm}$. To demonstrate this, we plot in Fig. 2(e) $P^{(2)}$ for photoelectron momenta indicated by filled green circles in Fig. 2(a). While each of these momenta by itself is symmetry-related to the momentum indicated by blue circles in Fig. 2(a), their sum (i.e., their center-of-mass momentum) is nonvanishing, $\mathbf{q}_{\rm cm} \neq 0$. As such, $P^{(2)}$ for these two momenta does not exhibit a zero-energy peak [see Fig. 2(e)] as the condensate possesses $\mathbf{q}_{\rm cm} = 0$. In contrast, the onset energy for the continuum, $\Delta\omega_c$ is still located at the same energy $2\Delta_{\mathbf{k}'_1}$ as in Fig. 2(b), as it arises from the breaking of two Cooper pairs.

Further, $P^{(2)}$ even reveals the spin-state of the Cooper pairs. In Fig. 2(f), we present $P^{(2)}$ for two photoelectrons with the same momenta as in Fig. 2(b) (filled blue circles), but possessing equal spins. In this case, $P^{(2)}$ does not exhibit a zero-energy peak (i.e., $P^{(2)}_{\rm sc} \equiv 0$), as the electrons in a Cooper pair form a spin-singlet state. Thus only a measurement of photoelectrons that are in opposite spin states will exhibit a zero-energy peak in $P^{(2)}$. In contrast, the continuum in $P^{(2)}_{\rm 2cp}$ is the same for equal and opposite spin states of the photoelectrons, as it arises from the breaking of two Cooper pairs. These results demonstrate that $2e$-ARPES experiments provide unprecedented insight into the center-of-mass

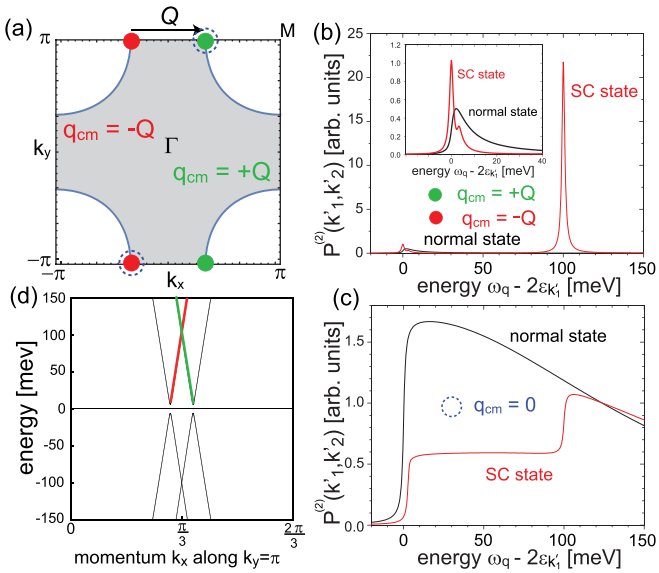

FIG. 3. (a) Schematic representation of superconducting pairing in the PDW phase, with $\mathbf{q}_{cm} = \pm\mathbf{Q}$. For the chosen electronic structure, we have $\mathbf{Q} = (2\pi/3, 0)$. (b) $P^{(2)}$ for photoelectrons with opposite spins and $\mathbf{q}_{cm} = \pm\mathbf{Q}$, as indicated by the sets of filled red and green circles in (a). The inset shows a zoom-in around $\Delta\omega = 0$. (c) $P^{(2)}$ for photoelectrons with opposite spins and opposite momenta, and hence $\mathbf{q}_{cm} = 0$, as indicated by the open blue circles in (a). (d) Electronic dispersion in the PDW phase as a function of k_x for $k_y = \pi$.

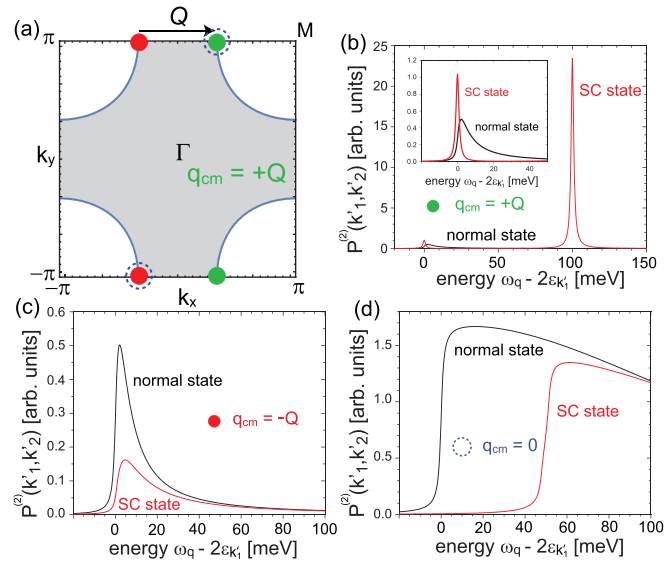

FIG. 4. (a) Schematic representation of superconducting pairing in the FFLO phase, with $\mathbf{q}_{cm} = +\mathbf{Q}$. $P^{(2)}$ for photoelectrons with opposite spins and (b) $\mathbf{q}_{cm} = +\mathbf{Q}$ [filled green circles in (a), the inset shows a zoom-in around $\Delta\omega = 0$], (c) $\mathbf{q}_{cm} = -\mathbf{Q}$ [filled red circles in (a)], and (d) $\mathbf{q}_{cm} = 0$ [open blue circles in (a)].

momentum and spin state of the superconducting condensate, as well as the momentum dependence of the superconducting order parameter.

To demonstrate the sensitivity of $2e$-ARPES experiments to detecting the center-of-mass momentum of Cooper pairs, we next consider two distinct superconducting phases with nonzero $\mathbf{q}_{cm}$. The first is the PDW phase, which has been proposed as a possible explanation for the puzzling phenomenology of the pseudogap region of the cuprate superconductors [7,19]. In this phase, electronic states with nonzero center-of-mass momentum $+\mathbf{Q}$ and $-\mathbf{Q}$ are simultaneously paired, with $\mathbf{Q}$ connecting the antinodal points near $(0, \pm\pi)$, as shown in Fig. 3(a). This leads to a pairing of states near $(\pm\mathbf{Q}/2, \pm\pi)$, such as the ones indicated by red (green) circles in Fig. 3(a) with center of mass momentum $\mathbf{q}_{cm} = \pm\mathbf{Q}$. For $P^{(2)}$ to directly probe the PDW condensate arising from this pairing, we need to select two photoelectrons with center-of-mass momentum $\mathbf{q}_{cm} = \pm\mathbf{Q}$ [red and green circles in Fig. 3(a)] as shown in Fig. 3(b). $P^{(2)}$ is identical for both sets of photoelectrons, exhibiting a peak at $\Delta\omega = 0$ that is separated by from the continuum by $2\Delta_{PDW}(\mathbf{k}'_{1,2})$. Similar to the case of a uniform $d_{x^2-y^2}$-wave superconductor discussed above, the peak at $\Delta\omega = 0$ directly reflects the existence of a PDW condensate with center of mass momentum $\mathbf{q}_{cm} = \pm\mathbf{Q}$. Thus, for photoelectrons with opposite momenta and zero center of mass momentum, as indicated by dashed blue circles in Fig. 3(a), $P^{(2)}$ does not exhibit a zero-energy peak, as shown in Fig. 3(c). We note that the continuum's peak in Fig. 3(b) is considerably higher than was the case for the uniform $d_{x^2-y^2}$-wave case discussed in Fig. 2. The reason for this large intensity is the electronic structure in the PDW phase near $\mathbf{k}'_{1,2} = (\mathbf{Q}/2, \pm\pi)$, shown in Fig. 3(d) where we plot the energy dispersion along k_x for $k_y = \pi$, i.e., perpendicular to the Fermi surface. As before, due to the momentum structure of the Coulomb interaction, the main contribution to $P^{(2)}$ arises from conduction electrons near $\mathbf{k}'_{1,2}$. The continuum peak arises from the breaking of two Cooper pairs, one of which is located on the red branch of the dispersion, and the other one on the green branch. Due to the linear dispersion near $\mathbf{k}'_{1,2}$, the energy required to break these two Cooper pairs is essentially constant and equal to $2\Delta_{PDW}$ over an extended range of k_x. This implies that, in contrast to the uniform $d_{x^2-y^2}$-wave case, for a fixed $\Delta\omega$ there is an extended momentum range of conduction electron states perpendicular to the Fermi surface that contribute to $P^{(2)}$, yielding the large continuum peak.

Finally, we consider the FFLO phase where the pairing occurs between states with a single nonzero center-of-mass momentum (strictly speaking, this corresponds to the Fulde-Ferrell phase [5]). While there currently is no evidence for an FFLO phase in the cuprate superconductors, the FFLO phase was reported [20] to occur in the heavy fermion $d_{x^2-y^2}$-wave superconductor $CeCoIn_5$ [21]. To allow explicit comparison with the results for a uniform $d_{x^2-y^2}$-wave superconductor (Fig. 2) and the PDW phase with $\mathbf{q}_{cm} = \pm\mathbf{Q}$ (Fig. 3), we choose for the FFLO phase $\mathbf{q}_{cm} = +\mathbf{Q}$. By assumption, then, pairing occurs between momentum states with $\mathbf{k}_1 + \mathbf{k}_2 = \mathbf{Q}$, represented by filled green circles in Fig. 4(a), but not between states with $\mathbf{k}_1 + \mathbf{k}_2 = -\mathbf{Q}$, as represented by filled red circles in Fig. 4(a). As expected, we find for the FFLO phase that $P^{(2)}$ exhibits a zero-energy peak for $\mathbf{k}'_1 + \mathbf{k}'_2 = \mathbf{Q}$ [green dots in Fig. 4(a)] that is separated from the continuum contribution by $2\Delta_{FFLO}$ [Fig. 4(b)]. In contrast, momentum states with $\mathbf{k}'_1 + \mathbf{k}'_2 = -\mathbf{Q}$, are unpaired and hence ungapped, such that

$P^{(2)}$ in the FFLO phase is simply suppressed in comparison to that in the normal state for these momenta. Furthermore, $P^{(2)}$ for these two momenta does not exhibit a zero-energy peak or a gap towards 2CP continuum excitations [Fig. 4(c)], in stark contrast to the PDW phase [Fig. 3(b)]. Interestingly, for photoelectrons with opposite momenta [dashed blue circles in Fig. 4(a)], $P^{(2)}$ again exhibits a gap towards 2CP continuum excitations, but its onset energy is shifted from that of the normal state only by Δ_{FFLO}, as only one of the momentum states is paired.

IV. CONCLUSIONS

We have developed a theory for the photoelectron counting rate $P^{(2)}$ measured in $2e$-ARPES experiments in a uniform $d_{x^2-y^2}$-wave superconducting, PDW and FFLO phases. A comparison of $P^{(2)}$ shown in Figs. 2–4 demonstrates that $2e$-ARPES measurements can identify the center-of-mass momentum (or even multiple center-of-mass momenta, as in the PDW phase), as well as the spin state of Cooper pairs, and thus distinguish between different superconducting pairing states. In addition, it is possible to map out the momentum dependence of the superconducting gap. $2e$-ARPES experiments thus provide a valuable new tool for the study of unconventional superconducting pairing states.

ACKNOWLEDGMENTS

This study was supported by the Center for Quantum Sensing and Quantum Materials, an Energy Frontier Research Center funded by the U. S. Department of Energy, Office of Science, Basic Energy Sciences under Award No. DE-SC0021238. P.A. acknowledges support from the EPiQS program of the Gordon and Betty Moore Foundation, Grant No. GBMF9452.

APPENDIX A: THEORETICAL FORMALISM

In the following, we provide more details regarding the derivation of the $2e$-ARPES photoelectron counting rate, $P^{(2)}$, arising from the process shown in Fig. 1(a). This process is described by the Hamiltonian of Eq.(1). The starting point for the calculation of $P^{(2)}$ is Eq. (3) with the initial and final states of the system defined in Eq. (2). For the calculation of $\hat{S}^{(2)}(\infty,-\infty)$, we note that there exists only single combination of scattering processes that connects $|\Psi_a\rangle$ and $|\Psi_b\rangle$ yielding

$$\hat{S}^{(2)}(\infty,-\infty)=\int_{-\infty}^{\infty}dt_1dt_2T\left[\sum_{\mathbf{k}_2,\mathbf{p},\mathbf{l}}\sum_{\sigma,\ \bar{\sigma}}V(\mathbf{l})d^{\dagger}_{\mathbf{k}_2+\mathbf{l},\ \bar{\sigma}}(t_1)d^{\dagger}_{\mathbf{p}-\mathbf{l},\sigma}(t_1)d_{\mathbf{p},\sigma}(t_1)c_{\mathbf{k}_2,\bar{\sigma}}(t_1)\sum_{\mathbf{k}_1,\sigma_1}\gamma_{\upsilon}(\mathbf{q})d^{\dagger}_{\mathbf{k}_1+\mathbf{q},\sigma_1}(t_2)c_{\mathbf{k}_1,\sigma_1}(t_2)a_{\mathbf{q},\upsilon}(t_2)\right]. \tag{A1}$$

Assuming that the photon beam is incident between times $-\Delta t/2\leqslant t\leqslant\Delta t/2$, we obtain

$$\begin{aligned}
&\langle\Psi_b|\hat{S}^{(2)}(\infty,-\infty)|\Psi_a\rangle\\
&=\langle\Psi_b|\int_{-\infty}^{\infty}dt_1dt_2T[\sum_{\mathbf{k}_2,\mathbf{p},\mathbf{l}}\sum_{\sigma,\ \bar{\sigma}}V(\mathbf{l})d^{\dagger}_{\mathbf{k}_2+\mathbf{l},\ \bar{\sigma}}(t_1)d^{\dagger}_{\mathbf{p}-\mathbf{l},\sigma}(t_1)d_{\mathbf{p},\sigma}(t_1)c_{\mathbf{k}_2,\bar{\sigma}}(t_1)\sum_{\mathbf{k}_1,\sigma_1}\gamma_{\upsilon}(\mathbf{q})d^{\dagger}_{\mathbf{k}_1+\mathbf{q},\sigma_1}(t_2)c_{\mathbf{k}_1,\sigma_1}(t_2)a_{\mathbf{q},\upsilon}(t_2)]|\Psi_a\rangle\\
&=\langle\Psi_b|\int_{-\Delta t/2}^{\Delta t/2}dt_2\int_{t_2}^{\infty}dt_1\sum_{\mathbf{k}_2,\mathbf{p},\mathbf{l}}\sum_{\sigma,\ \bar{\sigma}}V(\mathbf{l})d^{\dagger}_{\mathbf{k}_2+\mathbf{l},\ \bar{\sigma}}(t_1)d^{\dagger}_{\mathbf{p}-\mathbf{l},\sigma}(t_1)d_{\mathbf{p},\sigma}(t_1)c_{\mathbf{k}_2,\bar{\sigma}}(t_1)\sum_{\mathbf{k}_1,\sigma_1}\gamma_{\upsilon}(\mathbf{q})d^{\dagger}_{\mathbf{k}_1+\mathbf{q},\sigma_1}(t_2)c_{\mathbf{k}_1,\sigma_1}(t_2)a_{\mathbf{q},\upsilon}(t_2)|\Psi_a\rangle\\
&=\int_{-\Delta t/2}^{\Delta t/2}dt_2\int_{t_2}^{\infty}dt_1\sum_{\mathbf{k}_2,\mathbf{p},\mathbf{l}}\sum_{\sigma,\ \bar{\sigma}}V(\mathbf{l})\sum_{\mathbf{k}_1,\sigma_1}\gamma_{\upsilon}(\mathbf{q})\langle\Psi_b|d^{\dagger}_{\mathbf{k}_2+\mathbf{l},\ \bar{\sigma}}(t_1)d^{\dagger}_{\mathbf{p}-\mathbf{l},\sigma}(t_1)d_{\mathbf{p},\sigma}(t_1)c_{\mathbf{k}_2,\bar{\sigma}}(t_1)d^{\dagger}_{\mathbf{k}_1+\mathbf{q},\sigma_1}(t_2)c_{\mathbf{k}_1,\sigma_1}(t_2)a_{\mathbf{q},\upsilon}(t_2)|\Psi_a\rangle.
\end{aligned} \tag{A2}$$

Setting the photon momentum equal to zero with $\gamma_{\upsilon}(\mathbf{q})\to\gamma_0$ yields

$$\begin{aligned}
&\langle\Psi_b|d^{\dagger}_{\mathbf{k}_2+\mathbf{l},\ \bar{\sigma}}(t_1)d^{\dagger}_{\mathbf{p}-\mathbf{l},\sigma}(t_1)d_{\mathbf{p},\sigma}(t_1)c_{\mathbf{k}_2,\bar{\sigma}}(t_1)d^{\dagger}_{\mathbf{k}_1,\sigma_1}(t_2)c_{\mathbf{k}_1,\sigma_1}(t_2)a_{\mathbf{q},\upsilon}(t_2)|\Psi_a\rangle\\
&={}_{pe}\langle 1_{\mathbf{k}_2',\sigma_2'}1_{\mathbf{k}_1',\sigma_1'}|_p\langle 0|\langle\Phi_b|d^{\dagger}_{\mathbf{k}_2+\mathbf{l},\ \bar{\sigma}}(t_1)d^{\dagger}_{\mathbf{p}-\mathbf{l},\sigma}(t_1)d_{\mathbf{p},\sigma}(t_1)c_{\mathbf{k}_2,\bar{\sigma}}(t_1)d^{\dagger}_{\mathbf{k}_1,\sigma_1}(t_2)c_{\mathbf{k}_1,\sigma_1}(t_2)a_{\mathbf{q},\upsilon}(t_2)|\Phi_a\rangle|1_{\mathbf{q},\lambda}\rangle_p|0\rangle_{pe}\\
&=e^{-i\omega_{\mathbf{q}}t_2}e^{i\varepsilon_{\mathbf{k}_1}t_2}e^{i(-\varepsilon_{\mathbf{p}}+\varepsilon_{\mathbf{p}-\mathbf{l}}+\varepsilon_{\mathbf{k}_2+\mathbf{l}})t_1}{}_{pe}\langle 1_{\mathbf{k}_2',\sigma_2'}1_{\mathbf{k}_1',\sigma_1'}|_p\langle 0|\langle\Phi_b|d^{\dagger}_{\mathbf{k}_2+\mathbf{l},\ \bar{\sigma}}d^{\dagger}_{\mathbf{p}-\mathbf{l},\sigma}d_{\mathbf{p},\sigma}c_{\mathbf{k}_2,\bar{\sigma}}(t_1)d^{\dagger}_{\mathbf{k}_1,\sigma_1}c_{\mathbf{k}_1,\sigma_1}(t_2)a_{\mathbf{q},\upsilon}|\Phi_a\rangle|1_{\mathbf{q},\lambda}\rangle_p|0\rangle_{pe}\\
&=-e^{-i\omega_{\mathbf{q}}t_2}e^{i\varepsilon_{\mathbf{k}_1}t_2}e^{i(-\varepsilon_{\mathbf{p}}+\varepsilon_{\mathbf{p}-\mathbf{l}}+\varepsilon_{\mathbf{k}_2+\mathbf{l}})t_1}{}_{pe}\langle 1_{\mathbf{k}_2',\sigma_2'}1_{\mathbf{k}_1',\sigma_1'}|d^{\dagger}_{\mathbf{k}_2+\mathbf{l},\ \bar{\sigma}}d^{\dagger}_{\mathbf{p}-\mathbf{l},\sigma}d_{\mathbf{p},\sigma}d^{\dagger}_{\mathbf{k}_1,\sigma_1}|0\rangle_{pe}\,{}_p\langle 0|a_{\mathbf{q},\upsilon}|1_{\mathbf{q},\lambda}\rangle_p\langle\Phi_b|c_{\mathbf{k}_2,\bar{\sigma}}(t_1)c_{\mathbf{k}_1,\sigma_1}(t_2)|\Phi_a\rangle
\end{aligned} \tag{A3}$$

with $\omega_{\mathbf{q}}$ being the incident photon energy. We finally obtain

$$\begin{aligned}
&\langle\Psi_b|\hat{S}(\infty,-\infty)|\Psi_a\rangle\\
&=-\gamma_0\int_{-\Delta t/2}^{\Delta t/2}dt_2\int_{t_2}^{\infty}dt_1\sum_{\mathbf{k}_1,\mathbf{k}_2}\delta_{\mathbf{k}_1+\mathbf{k}_2-\mathbf{k}_1'-\mathbf{k}_2',0}\{V(\mathbf{k}_1-\mathbf{k}_2')\,e^{-i\omega_{\mathbf{q}}t_2}e^{i\varepsilon_{\mathbf{k}_1}t_2}e^{i(-\varepsilon_{\mathbf{k}_1}+\varepsilon_{\mathbf{k}_2'}+\varepsilon_{\mathbf{k}_1'})t_1}\langle\Phi_b|c_{\mathbf{k}_2,\sigma_2'}(t_1)c_{\mathbf{k}_1,\sigma_1'}(t_2)|\Phi_a\rangle\\
&\quad-V(\mathbf{k}_1-\mathbf{k}_1')\,e^{-i\omega_{\mathbf{q}}t_2}e^{i\varepsilon_{\mathbf{k}_1}t_2}e^{i(-\varepsilon_{\mathbf{k}_1}+\varepsilon_{\mathbf{k}_1'}+\varepsilon_{\mathbf{k}_2'})t_1}\langle\Phi_b|c_{\mathbf{k}_2,\sigma_1'}(t_1)c_{\mathbf{k}_1,\sigma_2'}(t_2)|\Phi_a\rangle\},
\end{aligned} \tag{A4}$$

where we used

$$
\begin{aligned}
&{}_p\langle 0|a_{\mathbf{q},\upsilon}|1_{\mathbf{q},\lambda}\rangle_p = 1,\\
&{}_{pe}\langle 1_{\mathbf{k}'_2,\sigma'_2}1_{\mathbf{k}'_1,\sigma'_1}|d^\dagger_{\mathbf{k}_2+\mathbf{l},\,\bar{\sigma}}d^\dagger_{\mathbf{p}-\mathbf{l},\sigma}d_{\mathbf{p},\sigma}d^\dagger_{\mathbf{k}_1,\sigma_1}|0\rangle_{pe}\\
&\quad=\left[\delta_{\mathbf{k}'_1,\mathbf{k}_2+\mathbf{l}}\delta_{\bar{\sigma},\sigma'_1}\delta_{\mathbf{k}'_2,\mathbf{p}-\mathbf{l}}\delta_{\sigma,\sigma'_2}-\delta_{\mathbf{k}'_1,\mathbf{p}-\mathbf{l}}\delta_{\sigma,\sigma'_1}\delta_{\mathbf{k}'_2,\mathbf{k}_2+\mathbf{l}}\delta_{\bar{\sigma},\sigma'_2}\right]\\
&\qquad\times\ \delta_{\mathbf{p},\mathbf{k}_1}\delta_{\sigma_1,\sigma}. \qquad \text{(A5)}
\end{aligned}
$$

To further evaluate the above term, we need to rewrite the term involving the fermionic annihilation operators using the respective Bogoliubov transformations for a uniform $d_{x^2-y^2}$-wave superconductor, the PDW and the FFLO phases, which we will consider in the following.

1. 2*e*-ARPES in a uniform $d_{x^2-y^2}$-wave superconductor with zero center-of mass momentum

a. $\mathbf{k}'_2=-\mathbf{k}'_1$ *and* $\sigma'_2\neq\sigma'_1$

For a uniform $d_{x^2-y^2}$-wave superconductor with zero center-of-mass momentum, the Bogoliubov transformation is given by

$$
\begin{aligned}
c_{-\mathbf{k}_2,\downarrow}&=-\upsilon_{\mathbf{k}_2}\alpha^\dagger_{\mathbf{k}_2}+u_{-\mathbf{k}_2}\beta_{-\mathbf{k}_2},\\
c_{\mathbf{k}_1,\uparrow}&=u_{\mathbf{k}_1}\alpha_{\mathbf{k}_1}+\upsilon_{-\mathbf{k}_1}\beta^\dagger_{-\mathbf{k}_1}. \qquad \text{(A6)}
\end{aligned}
$$

At $T=0$, the contribution to $P^{(2)}$ that directly reflects the presence of a superconducting condensate, $P^{(2)}_{\rm SC}$ [see Eq. (4) in the main text], arises from terms of the form

$$
\begin{aligned}
&\langle\Phi_b|\alpha_{\mathbf{k}}(t_1)\alpha^\dagger_{\mathbf{k}}(t_2)|\Phi_a\rangle,\\
&\langle\Phi_b|\beta_{\mathbf{k}}(t_1)\beta^\dagger_{\mathbf{k}}(t_2)|\Phi_a\rangle. \qquad \text{(A7)}
\end{aligned}
$$

Terms of these forms, however, can only emerge from Eq. (A4) if $\mathbf{k}_2=-\mathbf{k}_1$ and $\sigma'_1\neq\sigma'_2$. Since momentum conservation in Eq. (A4) requires that

$$\mathbf{k}_1+\mathbf{k}_2-\mathbf{k}'_1-\mathbf{k}'_2=0$$

this immediately implies $\mathbf{k}'_2=-\mathbf{k}'_1$, i.e., the center-of-mass momentum of the two photoelectrons is zero. Moreover, $\sigma'_1\neq\sigma'_2$ implies that the two photoelectrons are in a spin-singlet state. Thus, we obtain a nonzero $P^{(2)}_{\rm SC}$ contribution only if the center-of-mass momentum and the spin state of the two photoelectrons is the same as that of the condensate. We then obtain $P^{(2)}=P^{(2)}_{\rm SC}+P^{(2)}_{\rm 2cp}$, where

$$P^{(2)}_{\rm SC}=2\pi\,\delta\big(\omega_q-2\varepsilon_{\mathbf{k}'_1}\big)\frac{1}{Z}\sum_\alpha e^{-\beta E_\alpha}\langle\Phi_a||I(\mathbf{k}'_1)|^2|\Phi_a\rangle \qquad \text{(A8)}$$

and

$$
\begin{aligned}
I(\mathbf{k}'_1)&=\gamma_0\sum_{\mathbf{p}}V(\mathbf{k}'_1-\mathbf{p})\frac{\Delta_{\mathbf{p}}}{2E_{\mathbf{p}}}\\
&\quad\times\left[\frac{\hat{n}^\alpha_{\mathbf{p}}+\hat{n}^\beta_{\mathbf{p}}}{\omega_q+E_{\mathbf{p}}-\varepsilon_{\mathbf{p}}+i\delta}-\frac{1-\hat{n}^\alpha_{\mathbf{p}}+1-\hat{n}^\beta_{\mathbf{p}}}{\omega_q-E_{\mathbf{p}}-\varepsilon_{\mathbf{p}}+i\delta}\right] \qquad \text{(A9)}
\end{aligned}
$$

with $\hat{n}^\alpha_{\mathbf{p}}=\alpha^\dagger_{\mathbf{p}}\alpha_{\mathbf{p}}$ and $\hat{n}^\beta_{\mathbf{p}}=\beta^\dagger_{\mathbf{p}}\beta_{\mathbf{p}}$. Moreover, $E_{\mathbf{p}}=\sqrt{\xi^2_{\mathbf{p}}+\Delta^2_{\mathbf{p}}}$ ($\xi_{\mathbf{p}}$) is the electronic dispersion in the superconducting (normal) state. The normal state dispersion is given by

$$\xi_{\mathbf{p}}=-2t(\cos p_x+\cos p_y)-4t'\cos p_x\cos p_y-\mu \qquad \text{(A10)}$$

with $t'/t=-0.4$, $\mu/t=-0.5$, and $t=300$ meV, giving rise to the characteristic cuprate Fermi surface shown in Fig. 2(a). Moreover, the superconducting $d_{x^2-y^2}$-wave gap is given by

$$\Delta_{\mathbf{p}}=\frac{\Delta_0}{2}(\cos p_x-\cos p_y) \qquad \text{(A11)}$$

with $\Delta_0=25$ meV. At $T=0$, $P^{(2)}_{\rm SC}$ simplifies to the expression which is given in Eq. (4). Similarly, we obtain

$$
\begin{aligned}
P^{(2)}_{\rm 2cp}=2\pi\gamma_0^2\sum_{\mathbf{p}}\Bigg[&\delta\big(\omega_q-2\varepsilon_{\mathbf{k}'_1}-2E_{\mathbf{p}}\big)\left|\frac{V(\mathbf{k}'_1-\mathbf{p})}{\omega_q+E_{\mathbf{p}}-\varepsilon_{\mathbf{p}}+i\delta}\right|^2\upsilon^4_{\mathbf{p}}\big\langle\big(1-\hat{n}^\alpha_{\mathbf{p}}\big)\big(1-\hat{n}^\beta_{\mathbf{p}}\big)\big\rangle\\
&+\delta(\omega_q-2\varepsilon_{\mathbf{k}'_1}+2E_{\mathbf{p}})\left|\frac{V(\mathbf{k}'_1-\mathbf{p})}{\omega_q-E_{\mathbf{p}}-\varepsilon_{\mathbf{p}}+i\delta}\right|^2u^4_{\mathbf{p}}\big\langle\hat{n}^\alpha_{\mathbf{p}}\hat{n}^\beta_{\mathbf{p}}\big\rangle\Bigg], \qquad \text{(A12)}
\end{aligned}
$$

where $\upsilon^2_{\mathbf{p}}=[1-\xi_{\mathbf{p}}/E_{\mathbf{p}}]/$, and $u^2_{\mathbf{p}}=[1+\xi_{\mathbf{p}}/E_{\mathbf{p}}]/2$ are the superconducting coherence factors. At $T=0$, this result simplifies to the expression given in Eq. (4).

b. $\mathbf{k}'_2\neq\mathbf{k}'_1$ *and* $\sigma'_2\neq\sigma'_1$

We next consider the case where the two photoelectrons possess a nonzero center-of-mass momentum, i.e., $\mathbf{k}'_1+\mathbf{k}'_2=\mathbf{l}\neq0$, and opposite spins. In this case, $P^{(2)}_{\rm SC}\equiv0$, and $P^{(2)}_{\rm 2cp}=P^{(2)}_{\alpha\alpha}+P^{(2)}_{\alpha\beta}+P^{(2)}_{\beta\alpha}+P^{(2)}_{\beta\beta}$, where

$$
\begin{aligned}
P^{(2)}_{\alpha\alpha}&=2\pi\gamma_0^2\sum_{\mathbf{k}_1,\mathbf{k}_2}\delta_{\mathbf{k}_1+\mathbf{k}_2,\mathbf{l}}V^2(\mathbf{k}_1-\mathbf{k}'_2)\left|\frac{1}{\varepsilon_{\mathbf{k}'_1}+\varepsilon_{\mathbf{k}'_2}-\varepsilon_{\mathbf{k}_1}+E_{\mathbf{k}_2}+i\delta}+\frac{1}{\varepsilon_{\mathbf{k}'_1}+\varepsilon_{\mathbf{k}'_2}-\varepsilon_{\mathbf{k}_2}-E_{\mathbf{k}_1}+i\delta}\right|^2\upsilon^2_{\mathbf{k}_2}u^2_{\mathbf{k}_1}\big\langle n^\alpha_{\mathbf{k}_1}\big(1-n^\alpha_{\mathbf{k}_2}\big)\big\rangle\\
&\quad\times\delta\big(\varepsilon_{\mathbf{k}'_1}+\varepsilon_{\mathbf{k}'_2}-\omega_q-E_{\mathbf{k}_1}+E_{\mathbf{k}_2}\big),\\
P^{(2)}_{\alpha\beta}&=2\pi\gamma_0^2\sum_{\mathbf{k}_1,\mathbf{k}_2}\delta_{\mathbf{k}_1+\mathbf{k}_2,\mathbf{l}}V^2(\mathbf{k}_1-\mathbf{k}'_2)\left|\frac{1}{\varepsilon_{\mathbf{k}'_1}+\varepsilon_{\mathbf{k}'_2}-\varepsilon_{\mathbf{k}_1}-E_{\mathbf{k}_2}+i\delta}+\frac{1}{\varepsilon_{\mathbf{k}'_1}+\varepsilon_{\mathbf{k}'_2}-\varepsilon_{\mathbf{k}_2}-E_{\mathbf{k}_1}+i\delta}\right|^2u^2_{\mathbf{k}_2}u^2_{\mathbf{k}_1}\big\langle n^\alpha_{\mathbf{k}_1}n^\beta_{\mathbf{k}_2}\big\rangle\\
&\quad\times\delta\big(\varepsilon_{\mathbf{k}'_1}+\varepsilon_{\mathbf{k}'_2}-\omega_q-E_{\mathbf{k}_1}-E_{\mathbf{k}_2}\big),
\end{aligned}
$$

$$P^{(2)}_{\beta\alpha} = 2\pi\gamma_0^2 \sum_{\mathbf{k}_1,\mathbf{k}_2} \delta_{\mathbf{k}_1+\mathbf{k}_2,\mathbf{l}} V^2(\mathbf{k}_1-\mathbf{k}_2') \left| \frac{1}{\varepsilon_{\mathbf{k}_1'}+\varepsilon_{\mathbf{k}_2'}-\varepsilon_{\mathbf{k}_1}+E_{\mathbf{k}_2}+i\delta} + \frac{1}{\varepsilon_{\mathbf{k}_1'}+\varepsilon_{\mathbf{k}_2'}-\varepsilon_{\mathbf{k}_2}+E_{\mathbf{k}_1}+i\delta} \right|^2 v^2_{\mathbf{k}_2} v^2_{\mathbf{k}_1}$$
$$\times \left\langle \left(1-n^{\beta}_{\mathbf{k}_1}\right)\left(1-n^{\alpha}_{\mathbf{k}_2}\right)\right\rangle \delta\left(\varepsilon_{\mathbf{k}_1'}+\varepsilon_{\mathbf{k}_2'}-\omega_q+E_{\mathbf{k}_1}+E_{\mathbf{k}_2}\right),$$
$$P^{(2)}_{\beta\beta} = 2\pi\gamma_0^2 \sum_{\mathbf{k}_1,\mathbf{k}_2} \delta_{\mathbf{k}_1+\mathbf{k}_2,\mathbf{l}} V^2(\mathbf{k}_1-\mathbf{k}_2') \left| \frac{1}{\varepsilon_{\mathbf{k}_1'}+\varepsilon_{\mathbf{k}_2'}-\varepsilon_{\mathbf{k}_1}-E_{\mathbf{k}_2}+i\delta} + \frac{1}{\varepsilon_{\mathbf{k}_1'}+\varepsilon_{\mathbf{k}_2'}-\varepsilon_{\mathbf{k}_2}+E_{\mathbf{k}_1}+i\delta} \right|^2 v^2_{\mathbf{k}_1} u^2_{\mathbf{k}_2}$$
$$\times \left\langle n^{\beta}_{\mathbf{k}_2}\left(1-n^{\beta}_{\mathbf{k}_1}\right)\right\rangle \delta\left(\varepsilon_{\mathbf{k}_1'}+\varepsilon_{\mathbf{k}_2'}-\omega_q+E_{\mathbf{k}_1}-E_{\mathbf{k}_2}\right). \tag{A13}$$

c. Equal spin polarization of the photoelectrons, and $\mathbf{k}_2' = -\mathbf{k}_1'$

We next consider the case where the two photoelectrons possess equal spin polarization, and a zero center-of-mass momentum, i.e., $\mathbf{k}_2' = -\mathbf{k}_1'$. In this case, $P^{(2)} = P^{(2)}_{\alpha\alpha} + P^{(2)}_{\alpha\beta} + P^{(2)}_{\beta\beta}$, where

$$P^{(2)}_{\alpha\alpha} = 4\pi\gamma_0^2 \sum_{\mathbf{k}} \left[V(-\mathbf{k}_1'-\mathbf{k}) - V(\mathbf{k}_1'-\mathbf{k})\right]^2 \left| \frac{1}{\omega_q-\varepsilon_{\mathbf{k}}-E_{\mathbf{k}}+i\delta} \right|^2 u^4_{\mathbf{k}} \left\langle n^{\alpha}_{\mathbf{k}} n^{\alpha}_{-\mathbf{k}}\right\rangle \delta(\omega_q - 2\varepsilon_{\mathbf{k}_1'} + 2E_{\mathbf{k}}),$$
$$P^{(2)}_{\beta\beta} = 4\pi\gamma_0^2 \sum_{\mathbf{k}} \left[V(-\mathbf{k}_1'-\mathbf{k}) - V(\mathbf{k}_1'-\mathbf{k})\right]^2 \left| \frac{1}{\omega_q-\varepsilon_{\mathbf{k}}+E_{\mathbf{k}}+\delta} \right|^2 v^4_{\mathbf{k}} \left\langle \left(1-n^{\beta}_{\mathbf{k}}\right)\left(1-n^{\beta}_{-\mathbf{k}}\right)\right\rangle \delta(\omega_q - 2\varepsilon_{\mathbf{k}_1'} - 2E_{\mathbf{k}}),$$
$$P^{(2)}_{\alpha\beta} = 2\pi\gamma_0^2 \delta\left(\omega_q - 2\varepsilon_{\mathbf{k}_1'}\right) \sum_{\mathbf{k}} \left[V(-\mathbf{k}_1'-\mathbf{k}) - V(\mathbf{k}_1'-\mathbf{k})\right]^2 \left| \frac{1}{\omega_q-\varepsilon_{\mathbf{k}}-E_{\mathbf{k}}+i\delta} + \frac{1}{\omega_q-\varepsilon_{\mathbf{k}}+E_{\mathbf{k}}+i\delta} \right|^2$$
$$\times \left(\frac{\Delta_k}{2E_k}\right)^2 \left\langle \left(1-n^{\beta}_{\mathbf{k}}\right) n^{\alpha}_{\mathbf{k}}\right\rangle. \tag{A14}$$

Note that at $T = 0$, $P^{(2)}$ does not possess a contribution similar to $P^{(2)}_{\mathrm{SC}}$ in Eq. (4), as two photoelectrons with the same spin-projection cannot emerge from the same Cooper pair. For $T \neq 0$, $P^{(2)}_{\alpha\beta}$ exhibits a peak at $\Delta\omega = \omega_q - 2\varepsilon_{\mathbf{k}_1'} = 0$, similar to $P^{(2)}_{\mathrm{SC}}$ in Eq. (4) as the breaking of Cooper pairs by thermal excitations allows for the ejection of two electrons with equal spin at $\Delta\omega = 0$. However, for photoelectron momenta near the antinodal points, as considered in Fig. 2 of the main text, $P^{(2)}_{\alpha\beta}$ is exponentially suppressed $\sim \exp[-\Delta_{\mathbf{k}}/(k_B T)]$, and thus negligible at typical experimental temperatures due to the large superconducting gap in the cuprate superconductors.

2. 2*e*-ARPES in the FFLO phase

We next consider the photoelectron counting rate in the FFLO phase [5,6], where superconducting pairing occurs between two electrons with center-of-mass momentum $\mathbf{Q}$ (strictly speaking, this corresponds to the Fulde-Ferrell phase [5]), as described by the mean-field Hamiltonian

$$H = \sum_{\mathbf{k},\sigma} \xi_{\mathbf{k}} c^{\dagger}_{\mathbf{k},\sigma} c_{\mathbf{k},\sigma} - \sum_{\mathbf{k}} (\Delta_{\mathrm{FF}}(\mathbf{k}) c^{\dagger}_{\mathbf{k}+\mathbf{Q}/2,\uparrow} c^{\dagger}_{-\mathbf{k}+\mathbf{Q}/2,\downarrow}$$
$$+ \Delta_{\mathrm{FF}}(\mathbf{k}) c_{-\mathbf{k}+\mathbf{Q}/2,\downarrow} c_{\mathbf{k}+\mathbf{Q}/2,\uparrow}). \tag{A15}$$

Note that $\Delta_{\mathrm{FF}}(\mathbf{k})$ also depends on $\mathbf{Q}$, and in general needs to be self-consistently computed [22]. However, since we consider only photoelectron momenta near the antinodal points (see Fig. 4), and due the suppression of large momentum transfer due to the Coulomb interaction, we can neglect the detailed momentum dependence of the superconducting gap in the FF phase and simply set Δ_{FF} equal to a constant value, with $\Delta_{\mathrm{FF}} = 50\,\mathrm{meV}$.

To diagonalize the Hamiltonian, we next use the Bogoliubov transformation

$$c^{\dagger}_{\mathbf{k}+\mathbf{Q}/2,\uparrow} = u_{\mathbf{k}} \alpha^{\dagger}_{\mathbf{k}+\mathbf{Q}/2} + v_{\mathbf{k}} \beta_{-\mathbf{k}+\mathbf{Q}/2},$$
$$c_{-\mathbf{k}+\mathbf{Q}/2,\downarrow} = -v_{\mathbf{k}} \alpha^{\dagger}_{\mathbf{k}+\mathbf{Q}/2} + v_{\mathbf{k}} \beta_{-\mathbf{k}+\mathbf{Q}/2}, \tag{A16}$$

which yields

$$H = \sum_{\mathbf{k}} E^{\alpha}_{\mathbf{k}+\mathbf{Q}/2} \alpha^{\dagger}_{\mathbf{k}+\mathbf{Q}/2} \alpha_{\mathbf{k}+\mathbf{Q}/2} + E^{\beta}_{-\mathbf{k}+\mathbf{Q}/2} \beta^{\dagger}_{-\mathbf{k}+\mathbf{Q}/2} \beta_{-\mathbf{k}+\mathbf{Q}/2}, \tag{A17}$$

where

$$E^{\alpha}_{\mathbf{k}+\mathbf{Q}/2} = \sqrt{\left(\varepsilon^{+}_{\mathbf{k}}\right)^2 + \Delta^2_{\mathrm{FF}}(\mathbf{k})} + \varepsilon^{-}_{\mathbf{k}},$$
$$E^{\beta}_{-\mathbf{k}+\mathbf{Q}/2} = \sqrt{\left(\varepsilon^{+}_{\mathbf{k}}\right)^2 + \Delta^2_{\mathrm{FF}}(\mathbf{k})} - \varepsilon^{-}_{\mathbf{k}},$$
$$\varepsilon^{\pm}_{\mathbf{k}} = \frac{\varepsilon_{\mathbf{k}+\mathbf{Q}/2} \pm \varepsilon_{-\mathbf{k}+\mathbf{Q}/2}}{2}, \tag{A18}$$

and the coherence factor are given by

$$u_{\mathbf{k}} v_{\mathbf{k}} = \frac{\Delta_{\mathrm{FF}}(\mathbf{k})}{2\sqrt{\left(\varepsilon^{+}_{\mathbf{k}}\right)^2 + \Delta^2_{\mathrm{FF}}(\mathbf{k})}},$$
$$u^2_{\mathbf{k}} = \frac{1}{2}\left[1 + \frac{\varepsilon^{+}_{\mathbf{k}}}{\sqrt{\left(\varepsilon^{+}_{\mathbf{k}}\right)^2 + \Delta^2_{\mathrm{FF}}(\mathbf{k})}}\right],$$
$$v^2_{\mathbf{k}} = \frac{1}{2}\left[1 - \frac{\varepsilon^{+}_{\mathbf{k}}}{\sqrt{\left(\varepsilon^{+}_{\mathbf{k}}\right)^2 + \Delta^2_{\mathrm{FF}}(\mathbf{k})}}\right]. \tag{A19}$$

a. $\mathbf{k}'_1 + \mathbf{k}'_2 = \mathbf{Q}$

In order to obtain a nonzero $P^{(2)}_{\rm SC}$ in the FF phase, Eq. (A4) needs to contain terms of the form

$$\langle\Phi_b|\alpha_{\mathbf{k}+\mathbf{Q}/2}(t_1)\alpha^\dagger_{\mathbf{k}+\mathbf{Q}/2}(t_2)|\Phi_a\rangle,$$
$$\langle\Phi_b|\beta_{-\mathbf{k}+\mathbf{Q}/2}(t_1)\beta^\dagger_{-\mathbf{k}+\mathbf{Q}/2}(t_2)|\Phi_a\rangle, \tag{A20}$$

which together with momentum conservation

$$\mathbf{k} + \mathbf{Q}/2 + (-\mathbf{k} + \mathbf{Q}/2) - \mathbf{k}'_1 - \mathbf{k}'_2 = 0$$

implies $\mathbf{k}'_1 + \mathbf{k}'_2 = \mathbf{Q}$, requiring that the center-of-mass momentum of the two photoelectrons be $\mathbf{Q}$. In this case, we then obtain $P^{(2)} = P^{(2)}_{\rm SC} + P^{(2)}_{\rm 2cp}$, where

$$P^{(2)}_{\rm SC} = 2\pi\delta\big(\omega_{\mathbf{q}} - \varepsilon_{\mathbf{k}'_1} - \varepsilon_{\mathbf{k}'_2}\big)\frac{1}{Z}\sum_\alpha e^{-\beta E_\alpha}\big\langle\Psi^\alpha_s\big|\big|I(\mathbf{k}'_1)\big|^2\big|\Psi^\alpha_s\big\rangle \tag{A21}$$

and

$$I(\mathbf{k}'_1) = \gamma_0\sum_{\mathbf{p}} u_{\mathbf{p}}v_{\mathbf{p}}V(\mathbf{k}'_1 - (-\mathbf{p}+\mathbf{Q}/2))\Bigg[\frac{1-n^\beta_{-\mathbf{p}+\mathbf{Q}/2}}{\omega_{\mathbf{q}} - \varepsilon_{\mathbf{p}+\mathbf{Q}/2} - E^\beta_{-\mathbf{p}+\mathbf{Q}/2} - i\delta} + \frac{1-n^\alpha_{\mathbf{p}+\mathbf{Q}/2}}{\omega_{\mathbf{q}} - \varepsilon_{-\mathbf{p}+\mathbf{Q}/2} - E^\alpha_{\mathbf{p}+\mathbf{Q}/2} - i\delta}$$
$$-\frac{n^\alpha_{\mathbf{p}+\mathbf{Q}/2}}{\omega_{\mathbf{q}} - \varepsilon_{\mathbf{p}+\mathbf{Q}/2} + E^\alpha_{\mathbf{p}+\mathbf{Q}/2} - i\delta} - \frac{n^\beta_{-\mathbf{p}+\mathbf{Q}/2}}{\omega_{\mathbf{q}} - \varepsilon_{-\mathbf{p}+\mathbf{Q}/2} + E^\beta_{-\mathbf{p}+\mathbf{Q}/2} - i\delta}\Bigg]. \tag{A22}$$

Similarly, we obtain

$$P^{(2)}_{\rm 2cp} = 2\pi\gamma_0^2\sum_{\mathbf{p}} V^2(\mathbf{k}'_1 - (-\mathbf{p}+\mathbf{Q}/2))\Bigg\{\Bigg|\frac{1}{-\varepsilon_{\mathbf{p}+\mathbf{Q}/2} + \varepsilon_{\mathbf{k}'_2} + \varepsilon_{\mathbf{k}'_1} + E^\alpha_{\mathbf{p}+\mathbf{Q}/2} + i\delta} + \frac{1}{-\varepsilon_{-\mathbf{p}+\mathbf{Q}/2} + \varepsilon_{\mathbf{k}'_1} + \varepsilon_{\mathbf{k}'_2} + E^\beta_{-\mathbf{p}+\mathbf{Q}/2} + i\delta}\Bigg|^2$$
$$\times v^4_{\mathbf{p}}\big\langle\big(1-n^\beta_{-\mathbf{p}+\mathbf{Q}/2}\big)\big(1-n^\alpha_{\mathbf{p}+\mathbf{Q}/2}\big)\big\rangle\delta\big(\varepsilon_{\mathbf{k}'_2} + \varepsilon_{\mathbf{k}'_1} - \omega_q + E^\beta_{-\mathbf{p}+\mathbf{Q}/2} + E^\alpha_{\mathbf{p}+\mathbf{Q}/2}\big)$$
$$+\Bigg|\frac{1}{-\varepsilon_{\mathbf{p}+\mathbf{Q}/2} + \varepsilon_{\mathbf{k}'_2} + \varepsilon_{\mathbf{k}'_1} - E^\beta_{-\mathbf{p}+\mathbf{Q}/2} + i\delta} + \frac{1}{-\varepsilon_{-\mathbf{p}+\mathbf{Q}/2} + \varepsilon_{\mathbf{k}'_1} + \varepsilon_{\mathbf{k}'_2} - E^\alpha_{\mathbf{p}+\mathbf{Q}/2} + i\delta}\Bigg|^2$$
$$\times u^4_{\mathbf{p}}\big\langle n^\beta_{-\mathbf{p}+\mathbf{Q}/2}n^\alpha_{\mathbf{p}+\mathbf{Q}/2}\big\rangle\delta\big(\varepsilon_{\mathbf{k}'_2} + \varepsilon_{\mathbf{k}'_1} - \omega_q - E^\alpha_{\mathbf{p}+\mathbf{Q}/2} - E^\beta_{-\mathbf{p}+\mathbf{Q}/2}\big)\Bigg\}. \tag{A23}$$

b. $\mathbf{k}'_1 + \mathbf{k}'_2 \neq \mathbf{Q}$

We next consider the case when $\mathbf{k}'_1 + \mathbf{k}'_2 = \mathbf{l} \neq \mathbf{Q}$. In this case, we obtain $P^{(2)} = P^{(2)}_{\alpha\alpha} + P^{(2)}_{\alpha\beta} + P^{(2)}_{\beta\alpha} + P^{(2)}_{\beta\beta}$, where

$$P^{(2)}_{\alpha\alpha} = 2\pi\gamma_0^2\sum_{\mathbf{k}_1,\mathbf{k}_2}\delta_{\mathbf{k}_2,\mathbf{k}_1-\mathbf{l}+\mathbf{Q}}\Bigg|\frac{1}{-\varepsilon_{\mathbf{k}_1+\mathbf{Q}/2} + \varepsilon_{\mathbf{k}'_2} + \varepsilon_{\mathbf{k}'_1} + E^\alpha_{\mathbf{k}_2+\mathbf{Q}/2} + i\delta} + \frac{1}{-\varepsilon_{\mathbf{k}_2+\mathbf{Q}/2} + \varepsilon_{\mathbf{k}'_2} + \varepsilon_{\mathbf{k}'_1} - E^\alpha_{\mathbf{k}_1+\mathbf{Q}/2} + i\delta}\Bigg|^2$$
$$\times V^2(\mathbf{k}'_2 - \mathbf{k}_1 - \mathbf{Q}/2)\big(v_{\mathbf{k}_2}u_{\mathbf{k}_1}\big)^2\big\langle n^\alpha_{\mathbf{k}_1+\mathbf{Q}/2}(1-n^\alpha_{\mathbf{k}_2+\mathbf{Q}/2})\big\rangle\delta\big(\varepsilon_{\mathbf{k}'_2} + \varepsilon_{\mathbf{k}'_1} - \omega_q + E^\alpha_{\mathbf{k}_2+\mathbf{Q}/2} - E^\alpha_{\mathbf{k}_1+\mathbf{Q}/2}\big),$$

$$P^{(2)}_{\alpha\beta} = 2\pi\gamma_0^2\sum_{\mathbf{k}_1,\mathbf{k}_2}\delta_{\mathbf{k}_2,\mathbf{k}_1-\mathbf{l}+\mathbf{Q}}\Bigg|\frac{1}{-\varepsilon_{\mathbf{k}_1+\mathbf{Q}/2} + \varepsilon_{\mathbf{k}'_2} + \varepsilon_{\mathbf{k}'_1} + E^\alpha_{\mathbf{k}_2+\mathbf{Q}/2} + i\delta} + \frac{1}{-\varepsilon_{\mathbf{k}_2+\mathbf{Q}/2} + \varepsilon_{\mathbf{k}'_2} + \varepsilon_{\mathbf{k}'_1} + E^\beta_{-\mathbf{k}_1+\mathbf{Q}/2} + i\delta}\Bigg|^2$$
$$\times V^2(\mathbf{k}'_2 - \mathbf{k}_1 - \mathbf{Q}/2)\left(v_{\mathbf{k}_2}v_{\mathbf{k}_1}\right)^2\big\langle\big(1-n^\beta_{-\mathbf{k}_1+\mathbf{Q}/2}\big)\big(1-n^\alpha_{\mathbf{k}_2+\mathbf{Q}/2}\big)\big\rangle\delta\big(\varepsilon_{\mathbf{k}'_2} + \varepsilon_{\mathbf{k}'_1} - \omega_q + E^\alpha_{\mathbf{k}_2+\mathbf{Q}/2} + E^\beta_{-\mathbf{k}_1+\mathbf{Q}/2}\big),$$

$$P^{(2)}_{\beta\alpha} = 2\pi\gamma_0^2\sum_{\mathbf{k}_1,\mathbf{k}_2}\delta_{\mathbf{k}_2,\mathbf{k}_1-\mathbf{l}+\mathbf{Q}}\Bigg|\frac{1}{-\varepsilon_{\mathbf{k}_1+\mathbf{Q}/2} + \varepsilon_{\mathbf{k}'_2} + \varepsilon_{\mathbf{k}'_1} - E^\beta_{-\mathbf{k}_2+\mathbf{Q}/2} + i\delta} + \frac{1}{-\varepsilon_{\mathbf{k}_2+\mathbf{Q}/2} + \varepsilon_{\mathbf{k}'_2} + \varepsilon_{\mathbf{k}'_1} - E^\alpha_{\mathbf{k}_1+\mathbf{Q}/2} + i\delta}\Bigg|^2$$
$$\times V^2(\mathbf{k}'_2 - \mathbf{k}_1 - \mathbf{Q}/2)\left(u_{\mathbf{k}_2}u_{\mathbf{k}_1}\right)^2\langle n^\alpha_{\mathbf{k}_1+\mathbf{Q}/2}n^\beta_{-\mathbf{k}_2+\mathbf{Q}/2}\rangle\delta\big(\varepsilon_{\mathbf{k}'_2} + \varepsilon_{\mathbf{k}'_1} - \omega_q - E^\alpha_{\mathbf{k}_1+\mathbf{Q}/2} - E^\beta_{-\mathbf{k}_2+\mathbf{Q}/2}\big),$$

$$P^{(2)}_{\beta\beta} = 2\pi\gamma_0^2\sum_{\mathbf{k}_1,\mathbf{k}_2}\delta_{\mathbf{k}_2,\mathbf{k}_1-\mathbf{l}+\mathbf{Q}}\Bigg|\frac{1}{-\varepsilon_{\mathbf{k}_1+\mathbf{Q}/2} + \varepsilon_{\mathbf{k}'_2} + \varepsilon_{\mathbf{k}'_1} - E^\beta_{-\mathbf{k}_2+\mathbf{Q}/2} + i\delta} + \frac{1}{-\varepsilon_{\mathbf{k}_2+\mathbf{Q}/2} + \varepsilon_{\mathbf{k}'_2} + \varepsilon_{\mathbf{k}'_1} + E^\beta_{-\mathbf{k}_1+\mathbf{Q}/2} + i\delta}\Bigg|^2$$
$$\times V^2(\mathbf{k}'_2 - \mathbf{k}_1 - \mathbf{Q}/2)\left(u_{\mathbf{k}_2}v_{\mathbf{k}_1}\right)^2\big\langle\big(1-n^\beta_{-\mathbf{k}_1+\mathbf{Q}/2}\big)n^\beta_{-\mathbf{k}_2+\mathbf{Q}/2}\big\rangle\delta\big(\varepsilon_{\mathbf{k}'_2} + \varepsilon_{\mathbf{k}'_1} - \omega_q + E^\beta_{-\mathbf{k}_1+\mathbf{Q}/2} - E^\beta_{-\mathbf{k}_2+\mathbf{Q}/2}\big). \tag{A24}$$

3. 2*e*-ARPES in the PDW phase

We next consider the $2e$-ARPES photoelectron counting rate $P^{(2)}$ in the PDW phase, whose mean-field Hamiltonian is given by

$$H = \sum_{\mathbf{k}}{}' \left(c^\dagger_{\mathbf{k},\uparrow}, c^\dagger_{\mathbf{k}+\mathbf{Q},\uparrow}, c^\dagger_{\mathbf{k}-\mathbf{Q},\uparrow}, c_{-\mathbf{k},\downarrow}, c_{-\mathbf{k}+\mathbf{Q},\downarrow}, c_{-\mathbf{k}-\mathbf{Q},\downarrow}\right) \times \begin{pmatrix} \xi_{\mathbf{k}} & 0 & 0 & 0 & \Delta & \Delta \\ 0 & \xi_{\mathbf{k}+\mathbf{Q}} & 0 & \Delta & \Delta & 0 \\ 0 & 0 & \xi_{\mathbf{k}-\mathbf{Q}} & \Delta & 0 & \Delta \\ 0 & \Delta & \Delta & -\xi_{\mathbf{k}} & 0 & 0 \\ \Delta & \Delta & 0 & 0 & -\xi_{\mathbf{k}-\mathbf{Q}} & 0 \\ \Delta & 0 & \Delta & 0 & 0 & -\xi_{\mathbf{k}+\mathbf{Q}} \end{pmatrix} \times \begin{pmatrix} c_{\mathbf{k},\uparrow} \\ c_{\mathbf{k}+\mathbf{Q},\uparrow} \\ c_{\mathbf{k}-\mathbf{Q},\uparrow} \\ c^\dagger_{-\mathbf{k},\downarrow} \\ c^\dagger_{-\mathbf{k}+\mathbf{Q},\downarrow} \\ c^\dagger_{-\mathbf{k}-\mathbf{Q},\downarrow} \end{pmatrix} = \sum_{\mathbf{k}}{}' \Psi^\dagger_{\mathbf{k}} \hat{H}_{\mathbf{k}} \Psi_{\mathbf{k}}, \tag{A25}$$

where the primed sum runs over the Brillouin zone of the PDW phase. Here, $\Delta = \Delta_{\mathrm{PDW}}$ is the superconducting gap in the PDW phase which depends on $\mathbf{k}$ and $\mathbf{Q}$, and in general needs to be self-consistently computed. However, since in the main text, we consider only photoelectron momenta near the antinodal points (see Fig. 3), and due the suppression of large momentum transfer arising from the Coulomb interaction, we can neglect the detailed momentum dependence of the superconducting gap in the PDW phase and simply set Δ_{PDW} equal to a constant value, with $\Delta_{\mathrm{PDW}} = 50\,\mathrm{meV}$.

We next diagonalize the Hamiltonian using the unitary transformation

$$(c^\dagger_{\mathbf{k},\uparrow}, c^\dagger_{\mathbf{k}+Q,\uparrow}, c^\dagger_{\mathbf{k}-Q,\uparrow}, c_{-\mathbf{k},\downarrow}, c_{-\mathbf{k}+Q,\downarrow}, c_{-\mathbf{k}-Q,\downarrow}) = (\gamma^\dagger_{1,\mathbf{k}}, \gamma^\dagger_{2,\mathbf{k}}, \gamma^\dagger_{3\mathbf{k}}, \gamma^\dagger_{4,\mathbf{k},}, \gamma^\dagger_{5,\mathbf{k}}, \gamma^\dagger_{6,\mathbf{k}})\hat{U}^\dagger_{\mathbf{k}} = \Gamma^\dagger_{\mathbf{k}}\hat{U}^\dagger_{\mathbf{k}} \begin{pmatrix} c_{\mathbf{k},\uparrow} \\ c_{\mathbf{k}+Q,\uparrow} \\ c_{\mathbf{k}-Q,\uparrow} \\ c^\dagger_{-\mathbf{k},\downarrow} \\ c^\dagger_{-\mathbf{k}+Q,\downarrow} \\ c^\dagger_{-\mathbf{k}-Q,\downarrow} \end{pmatrix} = \hat{U} \begin{pmatrix} \gamma_{1,\mathbf{k}} \\ \gamma_{2,\mathbf{k}} \\ \gamma_{3\mathbf{k}} \\ \gamma_{4,\mathbf{k},} \\ \gamma_{5,\mathbf{k}} \\ \gamma_{6,\mathbf{k}} \end{pmatrix} = \hat{U}_{\mathbf{k}}\Gamma_{\mathbf{k}} \tag{A26}$$

with $\hat{U}$ being a unitary matrix consisting of the eigenvectors of $\hat{H}_{\mathbf{k}}$. Thus we obtain

$$H = \sum_{\mathbf{k}}{}' \Psi^\dagger_{\mathbf{k}} \hat{H}_{\mathbf{k}} \Psi_{\mathbf{k}} = \sum_{\mathbf{k}}{}' \Gamma^\dagger_{\mathbf{k}} \hat{U}^\dagger_{\mathbf{k}} \hat{H}_{\mathbf{k}} \hat{U}_{\mathbf{k}} \Gamma_{\mathbf{k}} = \sum_{\mathbf{k}}{}' \Gamma^\dagger_{\mathbf{k}} \hat{E}_{\mathbf{k}} \Gamma_{\mathbf{k}} \tag{A27}$$

with

$$\hat{E}_{\mathbf{k}} = \begin{pmatrix} E_{1,\mathbf{k}} & 0 & 0 & 0 & 0 & 0 \\ 0 & E_{2,\mathbf{k}} & 0 & 0 & 0 & 0 \\ 0 & 0 & E_{3,\mathbf{k}} & 0 & 0 & 0 \\ 0 & 0 & 0 & E_{4,\mathbf{k}} & 0 & 0 \\ 0 & 0 & 0 & 0 & E_{5,\mathbf{k}} & 0 \\ 0 & 0 & 0 & 0 & 0 & E_{6,\mathbf{k}} \end{pmatrix} \tag{A28}$$

and $E_{i,\mathbf{k}} (i = 1, \ldots, 6)$ are the eigenenergies of $\hat{H}_{\mathbf{k}}$.

a. $\mathbf{k}'_1 + \mathbf{k}'_2 = \pm\mathbf{Q}$

In this case, we obtain $P^{(2)} = P^{(2)}_{\mathrm{SC}} + P^{(2)}_{\mathrm{2cp}}$, where

$$P^{(2)}_{\mathrm{SC}} = 2\pi\delta(\omega_{\mathbf{q}} - \varepsilon_{k'_2} - \varepsilon_{k'_1}) \frac{1}{Z} \sum_{\alpha\beta} e^{-\beta E_\alpha} \left\langle \Psi^\alpha_s \middle| \left| I(\mathbf{k}'_1) \right|^2 \middle| \Psi^\alpha_s \right\rangle \tag{A29}$$

with

$$I(\mathbf{k}'_1) = \gamma_0 \sum_{\mathbf{p}} V(\mathbf{k}'_1 - (\mathbf{p} + \mathbf{Q})) \sum_{i=1,6} [\hat{U}_{\mathbf{p}}]_{5i} [\hat{U}_{\mathbf{p}}]_{1i} \times \left[\frac{n^{(i)}_F(\mathbf{p})}{\omega_q - \varepsilon_{\mathbf{p}} + E_{i,\mathbf{p}} + i\delta} - \frac{1 - n^{(i)}_F(\mathbf{p})}{\omega_q - \varepsilon_{\mathbf{p}} - E_{i,\mathbf{p}} + i\delta} \right] \tag{A30}$$

with $[\hat{U}_{\mathbf{p}}]_{ij}$ being the (ij) element of the matrix $\hat{U}_{\mathbf{p}}$, and

$$P^{(2)}_{\mathrm{2cp}} = 2\pi\gamma_0^2 \sum_{\mathbf{p}} V^2(\mathbf{k}'_1 - (-\mathbf{p} + \mathbf{Q})) \sum_{i \neq j} ([\hat{U}_{\mathbf{p}}]_{5i} [\hat{U}_{\mathbf{p}}]_{1j})^2 \times \left| \frac{1}{-\varepsilon_{\mathbf{p}} + \varepsilon_{\mathbf{k}'_2} + \varepsilon_{\mathbf{k}'_1} + E_{i,\mathbf{p}} + i\delta} + \frac{1}{-\varepsilon_{\mathbf{p}} + \varepsilon_{\mathbf{k}'_2} + \varepsilon_{\mathbf{k}'_1} - E_{j,\mathbf{p}} + i\delta} \right|^2 \times \delta(\varepsilon_{\mathbf{k}'_2} + \varepsilon_{\mathbf{k}'_1} - \omega_q + E_{i,\mathbf{p}} - E_{j,\mathbf{p}}) \times \left\langle \left(1 - n^{(i)}_F(\mathbf{p})\right) n^{(j)}_F(\mathbf{p}) \right\rangle. \tag{A31}$$

b. $\mathbf{k}'_1 + \mathbf{k}'_2 = \mathbf{0}$

In this case, we obtain

$$P^{(2)} = 2\pi\gamma_0^2 \sum_{\mathbf{p}} V^2(\mathbf{k}'_1 - \mathbf{p}) \sum_{i \neq j} ([\hat{U}_{\mathbf{p}}]_{4i} [\hat{U}_{\mathbf{p}}]_{1j})^2 \times \left| \frac{1}{\varepsilon_{\mathbf{k}'_1} + \varepsilon_{\mathbf{k}'_2} - \varepsilon_{\mathbf{p}} + E_{i,\mathbf{p}} + i\delta} + \frac{1}{\varepsilon_{\mathbf{k}'_1} + \varepsilon_{\mathbf{k}'_2} - \varepsilon_{\mathbf{p}} - E_{j,\mathbf{p}_1} + i\delta} \right|^2 \left\langle n^{(j)}_F(\mathbf{p}) \left(1 - n^{(i)}_F(\mathbf{p})\right) \right\rangle \times \delta(\varepsilon_{\mathbf{k}'_1} + \varepsilon_{\mathbf{k}'_2} - \omega_q + E_{i,\mathbf{p}} - E_{j,\mathbf{p}}). \tag{A32}$$

APPENDIX B: AUGER PROCESS CONTRIBUTION TO THE 2*e*-ARPES PHOTOELECTRON COUNTING RATE FOR A UNIFORM $d_{x^2-y^2}$-WAVE SUPERCONDUCTOR

We next consider the contribution to the $2e$-ARPES photoelectron counting rate involving the Auger process, $P^{(2)}_{\mathrm{Aug}}$, shown in Fig. 1(b) of the main text. In a uniform $d_{x^2-y^2}$-wave superconductor, for two photoelectrons with momenta

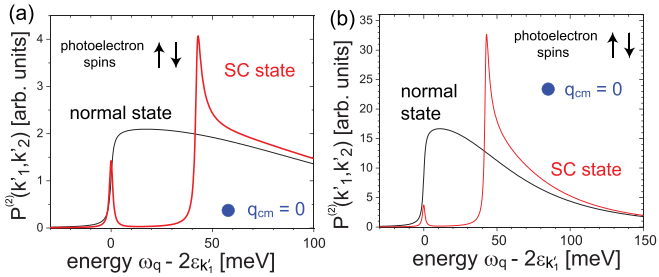

FIG. 5. $P^{(2)}$ in a uniform $d_{x^2-y^2}$-wave superconductor for two photoelectrons with $\mathbf{k}'_2 = -\mathbf{k}'_1$, $\sigma'_2 \neq \sigma'_1$, and momenta at the antinodal points [see filled blue circles in Fig. 2(a)] and two different screening lengths: (a) $\kappa^{-1} = 10a_0$ and (b) $20a_0$.

$\mathbf{k}'_2 = -\mathbf{k}'_1$ and opposite spin, $\sigma'_2 \neq \sigma'_1$, we obtain at $T = 0$

$$P^{(2)}_{\mathrm{Aug}} = 8\pi\delta(2\varepsilon_{\mathbf{k}'_1} - \omega_q)\langle n^f_{\mathbf{k}'_1}\rangle\gamma_0^2\left|\frac{1}{\varepsilon_{\mathbf{k}'_1} + \zeta_{\mathbf{k}'_1} + i\delta}\right|^2 \times \left|\sum_{\mathbf{p}} U(\mathbf{p} - \mathbf{k}'_1)\frac{\Delta_{\mathbf{p}}}{2E_{\mathbf{p}}}\right|^2 + 8\pi\gamma_0^2\langle n^f_{\mathbf{k}'_1}\rangle \times \sum_{\mathbf{p}} \delta\big(2\varepsilon_{\mathbf{k}'_1} - \omega_q + 2E_{\mathbf{p}}\big)v_{\mathbf{p}}^4\left|\frac{U(\mathbf{p} - \mathbf{k}'_1)}{\varepsilon_{\mathbf{k}'_1} + \zeta_{\mathbf{k}'_1} + 2E_{\mathbf{p}} + i\delta}\right|^2, \tag{B1}$$

where $\zeta_{\mathbf{k}'_1}$ is the energy of the core state electron, $\langle n^f_{\mathbf{k}'_1}\rangle$ is the occupation of the core electron state, and $U(\mathbf{p} - \mathbf{k}'_1)$ is the interaction describing the Auger process. $P^{(2)}_{\mathrm{Aug}}$ possesses the same structure as the result shown in Eq. (4), albeit with different weighting factors. Note that the calculation of $P^{(2)}_{\mathrm{Aug}}$ thus requires knowledge of the detailed momentum and energy structure of the core levels, and that $P^{(2)}_{\mathrm{Aug}}$ is only nonzero if there exist occupied core electron states with the same momenta as those of the two photoelectrons probed in the detectors.

APPENDIX C: EFFECT OF A SCREENED COULOMB INTERACTION ON THE PHOTOELECTRON COUNTING RATE IN A UNIFORM $d_{x^2-y^2}$-WAVE SUPERCONDUCTOR

As discussed above, the momentum dependence of the Coulomb interaction is crucial for the observation of a nonzero $P^{(2)}_{\mathrm{SC}}$ due to the momentum structure of the superconducting order parameter. One might therefore wonder how a change in the screening length κ^{-1} of the Coulomb interaction, $V(\mathbf{q}) = V_0/(\mathbf{q}^2 + \kappa^2)$ affects the energy dependence of $P^{(2)}$. To investigate this question, we computed $P^{(2)}$ for two photoelectrons with zero center-of-mass momentum, i.e., $\mathbf{k}'_2 = -\mathbf{k}'_1$, and opposite spin polarization, i.e., $\sigma'_2 \neq \sigma'_1$, in a uniform $d_{x^2-y^2}$-wave superconductor, for two different screening length, as shown in Fig. 5. While the qualitative structure of $P^{(2)}$ does not change with increasing κ^{-1}, albeit with an overall intensity increase, we find that the relative height between the peaks arising from $P^{(2)}_{\mathrm{SC}}$ and $P^{(2)}_{\mathrm{2cp}}$ decreases with increasing κ^{-1}. We remind, however, that $P^{(2)}_{\mathrm{SC}}$ and $P^{(2)}_{\mathrm{2cp}}$ are scaled with overall factors of $(4\pi^2/N)^2$ and $4\pi^2/N$, respectively, such that even an increase in κ^{-1} will not significantly affect the much larger intensity of the peak in $P^{(2)}_{\mathrm{SC}}$.

[1] P. Abbamonte, E. Demler, J. C. S. Davis, and J.-C. Campuzano, Resonant soft x-ray scattering, stripe order, and the electron spectral function in cuprates, Physica C **481**, 15 (2012).

[2] A. Damascelli, Z. Hussain, and Z.-X. Shen, Angle-resolved photoemission studies of the cuprate superconductors, Rev. Mod. Phys. **75**, 473 (2003).

[3] D. J. V. Harlingen, Phase-sensitive tests of the symmetry of the pairing state in the high-temperature superconductors–evidence for $d_{x^2-y^2}$-symmetry, Rev. Mod. Phys. **67**, 515 (1995).

[4] C. C. Tsuei and J. R. Kirtley, Pairing symmetry in cuprate superconductors, Rev. Mod. Phys. **72**, 969 (2000).

[5] P. Fulde and R. A. Ferrell, Superconductivity in a strong spin-exchange field, Phys. Rev. **135**, A550 (1964).

[6] A. I. Larkin and Y. N. Ovchinnikov, Nonuniform state of superconductors, Sov. Phys. JETP **20**, 762 (1965).

[7] E. Berg, E. Fradkin, S. A. Kivelson, and J. M. Tranquada, Striped superconductors: How spin, charge and superconducting orders intertwine in the cuprates, New J. Phys. **11**, 115004 (2009).

[8] J. Berakdar, Emission of correlated electron pairs following single-photon absorption by solids and surfaces, Phys. Rev. B **58**, 9808 (1998).

[9] B. D. Napitu and J. Berakdar, Two-particle photoemission from strongly correlated systems: A dynamical mean-field approach, Phys. Rev. B **81**, 195108 (2010).

[10] H.W. Haak, G. A. Sawatzky, and T. D. Thomas, Auger-Photoelectron Coincidence Measurements in Copper, Phys. Rev. Lett. **41**, 1825 (1978).

[11] C.-T. Chiang, A. Trützschler, M. Huth, R. Kamrla, F. O. Schumann, and W. Widdra, Laser-based double photoemission spectroscopy at surfaces, Prog. Surf. Sci. **95**, 100572 (2020).

[12] N. Fominykh, J. Berakdar, J. Henk, and P. Bruno, Spectroscopy of the Electron-Electron Interaction in Solids, Phys. Rev. Lett. **89**, 086402 (2002).

[13] F. O. Schumann, C. Winkler, and J. Kirschner, Correlation Effects in Two Electron Photoemission, Phys. Rev. Lett. **98**, 257604 (2007).

[14] F. O. Schumann, R. S. Dhaka, G. A. van Riessen, Z. Wei, and J. Kirschner, Surface state and resonance effects in electron-pair emission from Cu(111), Phys. Rev. B **84**, 125106 (2011).

[15] F. O. Schumann, L. Behnke, C. H. Li, J. Kirschner, Y. Pavlyukh, and J. Berakdar, Electron pair emission from a highly correlated material, Phys. Rev. B **86**, 035131 (2012).

[16] R. Herrmann, S. Samarin, H. Schwabe, and J. Kirschner, Two Electron Photoemission in Solids, Phys. Rev. Lett. **81**, 2148 (1998).

[17] Y. Pavlyukh, M. Schüler, and J. Berakdar, Single- or double-electron emission within the keldysh nonequilibrium green's function and feshbach projection operator techniques, Phys. Rev. B **91**, 155116 (2015).

[18] K. A. Kouzakov and J. Berakdar, Photoinduced Emission of Cooper Pairs from Superconductors, Phys. Rev. Lett. **91**, 257007 (2003).

[19] D. F. Agterberg, J. S. Davis, S. D. Edkins, E. Fradkin, D. J. Van Harlingen, S. A. Kivelson, P. A. Lee, L. Radzihovsky, J. M. Tranquada, and Y. Wang, The physics of pair-density waves: Cuprate superconductors and beyond, Annu. Rev. Condens. Matter Phys. **11**, 231 (2020).

[20] A. Bianchi, R. Movshovich, C. Capan, P. G. Pagliuso, and J. L. Sarrao, Possible Fulde-Ferrell-Larkin-Ovchinnikov Superconducting State in $CeCoIn_5$, Phys. Rev. Lett. **91**, 187004 (2003).

[21] M. P. Allan, F. Massee, D. K. Morr, J. V. Dyke, A. W. Rost, A. P. Mackenzie, C. Petrovic, and J. C. Davis, Imaging cooper pairing of heavy fermions in $CeCoIn_5$, Nat. Phys. **9**, 468 (2013).

[22] M. Graham and D. K. Morr, Josephson Scanning Tunneling Spectroscopy in $d_{x^2-y^2}$-Wave Superconductors: A Probe for the Nature of the Pseudogap in the Cuprate Superconductors, Phys. Rev. Lett. **123**, 017001 (2019).